Chalcogenide Letters Vol. 19, No. 2, February 2022, p. 103 - 116

Effect of annealing time on the structural, morphological, optical and electrical properties of NiS thin films

A. Gahtar[a, b,*], A. Benali[a], S. Benramache[b], C. Zaouche[b]
[a]*Department of biology, Faculty of sciences, University Elchahid Hamma Lakhder, 39000 El Oued, Algeria*
[b]*Material Sciences Department, Faculty of Sciences, University of Biskra, 07000, Algeria*

In this work, we prepared thin films of nickel sulfide by spray pyrolysis on substrates of the glass at temperature of 300°C. The solution used is a mixture of nickel acetate and thiourea as a source of nickel and sulfur respectively, acetic acid was used as a complexing agent, and then heated the resulting layers in an ordinary furnace at 300°C at different times of 1h, 2h and 3h to study the annealing time effect on the physical and chemical properties. The characterization methods used indicate remarkable changes in the structural, electrical, morphological and optical properties of NiS films under annealing time. The results obtained have shown that the prepared NiS films contain good crystallization, dense morphology, good stochiometric ratio and high conductivity, and these specifications make them a potential candidate as electrode material for application in super-capacitors.

(Received November 7, 2021; Accepted February 11, 2022)

Keywords: Nickel sulfide, spray-pyrolysis, Annealing time, DRX, SEM&EDS

1. Introduction

Nickel sulfide is the most attractive material since it has high electron mobility, a good reflection in the infrared range, an ease of production and low toxicity. As one of the main classes of transition metals, Chalcogénures, nickel sulfides exist in different phases, such as NiS, NiS_2, Ni_3S_2, Ni_7S_6 and Ni_9S_8. Among these phases, NiS exhibits an excellent capacity performance, high redox activity, which should satisfy the growing need for energy storage systems [1]. Scientists think that this material is important and challenging. Generally, NiS exists in two phases, hexagonal and rhombohedral [2]. Both phases exhibit a many applications. Different methods such as spray pyrolysis [3] the deposition of the chemical bath (CBD) [4], hydrothermal [5], adsorption and reaction of successive ionic layer (SILAR)[6], thermal evaporation [7], electro-deposition [8] and sol-gel [9] have deposited the thin films of NiS. Since thin films are very important in industrial production, an easy and inexpensive method should be sought among the methods which have proven to be effective are the spray pyrolysis method, because they do not require advanced technologies and complex devices, but they need simple devices and access to films at low cost. These films deposited in this way are characterized by their strong adhesion to the substrate, the ability to prepare a film with surfaces relatively large and the ability to obtain films with the required specifications, and this is done by mixing a solution of two or more materials and changing the proportions involved in the composition of the film.

In this article, we describe the preparation method, the experimental details and techniques that describe the layers deposited with NiS. Then we discuss the results obtained of the prepared NiS. Finally, a summary of the research will be given and prospects for future research will be discussed.

* Corresponding author: abdelouahab-gahtar@univ-eloued.dz
https://doi.org/10.15251/CL.2022.192.103

2. Experimental details

2.1. Preparation of nickel sulfide NiS films

We used nickel sulfide NiS films prepared by pyrolysis spraying on glass substrates, nickel acetate (($C_4H_6O_4Ni$. $4H_2O$), 0.07 mol/l) was used as a source of Ni, thiourea ($CS(NH_2)_2$, 0.21mol/l) was used as a source of S and acetic acid was used as a complexing agent. The cleaned glass substrates were heated to (300±5) °C on a hot plate. The distance between the nozzle and the substrate was chosen at 40 cm and air pressure of 0.5 bar was used as carrier gas, the flow rate of the solution was adjusted to 10 ml/min. using a flow meter and the atomization process was completed in about 15 minutes. In addition to pure NiS, we prepared series of thin film NiS annealed in an ordinary furnace at temperature Tr=300 °C with different annealing times of 1h ,2h and 3h.

One of the initial fundamental steps needed to reduce the potential site for interface recombination in thin films is to ensure the use of clean substrates for deposition. In this study, soda lime glass slides with the dimensions: 76 mm × 26 mm, were used as substrates. The soda lime glasses were first cleaned using detergent and with distilled water. Further, the glass substrates were then cleaned ultrasonically for 15 minutes, followed by a rinse with acetone and the glass substrates were then dried by using nitrogen gas. Our study focused on four types of samples presented in Table1.

Table 1. Symbols of the different NiS films prepared by the technique of the spray pyrolysis on glass substrates at 300 °C then heat treatment at 300 °C in an ordinary oven at different times 1 h, 2 h and 3h.

Samples	Film preparation conditions
(a): 0h	Thin film of NiS deposited by spray pyrolysis at 300 ° C not annealed
(b): 1h	Thin film of NiS deposited by spray pyrolysis at 300 ° C and heat treated in an oven at 300 ° C for 1 hour
(c): 2h	Thin film of NiS deposited by spray pyrolysis at 300 ° C and heat treated in an oven at 300 ° C for 2 hour
(d): 3h	Thin film of NiS deposited by spray pyrolysis at 300 ° C and heat treated in an oven at 300 ° C for 3 hour

The film thickness was estimated using the weight method, which yields the thickness according to the formula [10]:

$$e = \frac{m}{\rho * S} \tag{1}$$

where e is the film thickness, m the mass deposited onto substrate, S the area of the film and ρ is the density of NiS (5.50 g/cm^3 [11]).

2.2. Characterization techniques

The thin films obtained NiS unannealed and annealed 1h, 2h and 3h were characterized by: Phase compositions of the films were obtained from the data of the X-ray diffractograms (XRD) using X-ray diffraction analysis (Bruker/D8). Cu Kα radiation target of wavelength 0.154 nm was employed in the 2θ range from 20º to 60º at room temperature. A dual-beam UV-visible spectrophotometer (UV-3101; Shimadzu), was used to measure the transmittance and reflectance in the wavelength range of 300 – 1100 nm with a resolution of 5 nm. The surface morphology was analyzed using an electron microscopy scanning (SEM; Qanta 350) equipped with an energy dispersive spectrometer (EDS) for elementary analysis. The type of chemical bonds present in the samples was identified using an infrated transmission spectrometer (FTIR; Shimadzu, model IR

Affinity-1) in the range of 400-4000 cm^{-1}. The electrical measurements were recorded using the four-probe method.

3. Results and discussion

3.1. X-Ray Diffraction

Fig.1 shows the X-ray diffraction (XRD) spectra of unannealed and annealed 1h, 2h and 3h NiS samples deposited on glass substrates by the spray pyrolysis technique at temperatures of 300°C.

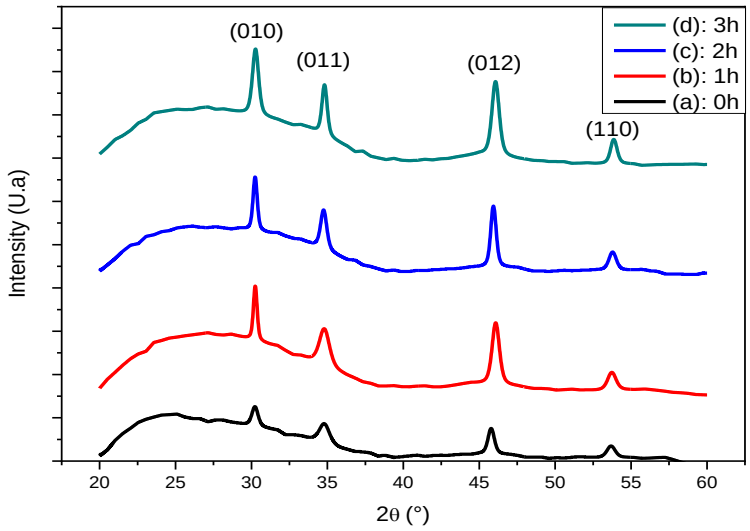

Fig. 1. DRX spectra of the NiS films: (a): 0h, (b): 1h, (c): 2h and (d): 3h.

The DRX spectra show that all the thin films obtained are polycrystalline and have a hexagonal structure strongly oriented in the (012) directions, on the unannealed and annealed NiS spectrum we notice the presence of diffraction peaks corresponding respectively to the : (010); (011); (012); (110) of polycrystalline NiS of hexagonal structure (JCPDS card # 98-064-6340). We also note that the peaks are slightly offset from the positions shown on the ASTM Data Sheet. This shift is probably due to stresses that deform the mesh, which has led to changes in the mesh parameters that more or less shift the position of the peaks as shown in Table 3. On the other side of the coin, the data obtained in this study are also in a good agreement with the previous reports in the literature on NiS films prepared by spray-pyrolysis and other techniques [3, 12, 13].

The unit cell parameters a, b and c, were determined using the following formula [14]:

$$\frac{1}{d_{hkl}^2} = \frac{3}{4}\left(\frac{h^2+k^2+hk}{a^2}\right) + \frac{l^2}{c^2} \quad (2)$$

The unit cell volume was evaluated using the following formula:

$$V = a^2 \times c \times sin(60^\circ) \quad (3)$$

Table 2. Lattice parameters (a, b and c) and the unit cell volume V compared to those values of the JCPDS card #98-064-6340.

Annealing time	Latice parameters						Unit cell volume ($Å^3$)
	Our data			JCPDS card			
	a=b (Å)	c (Å)	c/a	a=b (Å)	c (Å)	c/a	
(a): 0h	3.416	5.275	1.544	3.420	5.300	1.550	52.936
(c): 1h	3.411	5.284	1.549				52.871
(d): 2h	3.413	5.266	1.542				52.753
(b): 3h	3.413	5.282	1.547				52.913

Table 2 resumes the obtained values of the structural parameters compared to those of the corresponding JCPDS card. It is observed that the reported values of the films are very close to each others. Furthermore, the unit cell volume decreases with the increase in the annealing time, owing to an improved crystal growth in the films [14]. This phenomenon shows that the annealing of the resulting layers has an essential role in the improvement of optical quality and electrical properties [15]. Table 3 summarizes the inter-plans distances determined from the XRD patterns. The observed mismatch between the inter-plans distances indicates the formation of strained lattice with the development of micro-stress during crystallization of the films.

The inter-plans distance (d_{hkl}) was calculated by Bragg formula [16, 17]:

$$2dd_{hkl} \sin\theta = n\lambda \tag{4}$$

Table 3. Inter-planar distances (d_{hkl}) of NiS thin films.

Annealing time	(a): 0h	(c): 1h	(d): 2h	(b): 3h
d_{010} (Å)	2,959	2,957	2,958	2,955
d_{011} (Å)	2,580	2,580	2,583	2,579
d_{012} (Å)	1,983	1,971	1,977	1,972
d_{110} (Å)	1,709	1,707	1,706	1,703

X-ray diffraction spectra were exploited to determine the crystallites size D, dislocation density δ and stresses ε in NiS films.

Firstly, The crystallite size (D_{hkl}) was estimated for all diffraction peaks using Scherer formula [18]:

$$D_{hkl} = \frac{k\lambda}{\beta_{1/2}\cos\theta} \tag{5}$$

where: k is a constant (k = 0.90), $\beta_{1/2}$ the full width at half maximum of the diffraction peak, θ is the Bragg angle and λ= 1.5406 Å is the wavelength of the X-ray radiation used.

Table 4. The crystallites size (D_{hkl}) of NiS thin films.

Annealing time	(a): 0h	(c): 1h	(d): 2h	(b): 3h
D_{010} (nm)	18,680	32,025	28,018	18,682
D_{011} (nm)	11,338	11,338	18,896	22,678
D_{012} (nm)	19,573	16,796	23,500	16,795

D_{110} (nm)	15,154	15,157	17,329	20,223

Secondly, The dislocation density (δ_{hkl}), which measures the amount of defects in a crystal is defined by the length of dislocation lines per unit volume. We used the following formula in order to determine it [10, 13]:

$$\delta_{hkl} = \frac{1}{D_{hkl}^2} \tag{6}$$

Table 5. The dislocation density (δ_{hkl}) of NiS thin films.

Annealing time	(a): 0h	(c): 1h	(d): 2h	(b): 3h
δ_{010} (10^{15} lines/ m^2)	2.872	0.975	1.271	2.875
δ_{011} (10^{15} lines/ m^2)	7.788	7.784	2.806	1.944
δ_{012} (10^{15} lines/ m^2)	2.614	3.543	1.814	3.541
δ_{110} (10^{15} lines/ m^2)	4.351	4.351	3.337	2.456

Finally, the microstrain (ε_{hkl}), was estimated using the following formula [19]:

$$\varepsilon_{hkl} = \frac{\beta_{1/2}}{4\tan\theta} \tag{7}$$

Table 6. Micro-stress values (ε_{hkl}) of NiS thin films.

Annealing time	(a): 0h	(c): 1h	(d): 2h	(b): 3h
ε_{010} (10^{-3})	7.636	4.451	5.089	7.626
ε_{011} (10^{-3})	10.97	10.993	6.591	5.482
ε_{011} (10^{-3})	4.885	5.657	4.056	5.659
ε_{110} (10^{-3})	5.436	5.430	4.745	4.060

Else ways, The texture coefficient (TC_{hkl}), which is calculated in terms of the intensity of each orientation (I_{hkl}) to the corresponding intensity of the JCPDS card (I_{0hkl}), gives information on the probability of the growth according to an orientation [hkl]. The coefficient (TC_{hkl}) is given by relation below [20]:

$$TC_{hkl} = \frac{I_{hkl}/I_{0\,hkl}}{N^{-1}\left(\sum_{i=1}^{n}\frac{I_{hkl}}{I_{0\,hkl}}\right)} \tag{8}$$

where: N is the number of diffraction peaks. The obtained values of TC_{hkl} are gathered in Table 7. As we can see, the value of the largest texture coefficient with respect to all the films corresponds to the peak (012), which indicates that it is the preferred orientation. Hence, the peak (012) has the highest intensity when compared to the other peaks. The crystallites are predominantly parallel to the plane of the substrate.

Table 7. Texture coefficient (TC_{hkl}) of NiS thin films prepared at diferent annealing time.

Annealing time	(a): 0h	(c): 1h	(d): 2h	(b): 3h
TC_{010}	0,992	1,292	1,332	1,212
TC_{011}	1,112	0,847	0,807	0,936

TC_{012}	1,385	1,444	1,540	1,383
TC_{110}	0,509	0,415	0,318	0,466

The average crystallites size $\prec D \succ$, average micro-stress $\prec \varepsilon \succ$ and the average dislocation density $\prec \delta \succ$ of the films, can be determined using the formulas below [19,21, 22]:

$$\langle D \rangle = \frac{\sum TC_{hkl} * D_{hkl}}{n} \tag{9}$$

$$\langle \varepsilon \rangle = \frac{\sum TC_{hkl} * \varepsilon_{hkl}}{n} \tag{10}$$

$$\langle \delta \rangle = \frac{\sum TC_{hkl} * \delta_{hkl}}{\sum TC_{hkl}} \tag{11}$$

Table 8. The average values of D, ε and δ of NiS films prepared with Annealing time.

Annealing time	$\prec D \succ$ (nm)	$\prec \varepsilon \succ \left(10^{-3}\right)$	$\prec \delta \succ$ (10^{15} lines/m^2)
(a): 0h	16.498	7.330	4,336
(c): 1h	20.391	6.369	3,703
(d): 2h	23.584	4.967	1,951
(b): 3h	19.145	6.027	2,848

It is evident that the micro-stress and the dislocation density decrease with increasing annealing time, inferring the formation of high quality thin films [23]. Acoordingly, the average crystallites size increases. This may be due to the fact that small crystallites are consumed during crystallization. Whereas, the dislocations acquire more energy and exhibit higher mobility. These dislocations that are activated segregate towards the boundaries of grains and are neutralized as the crystallization of the film proceeds [24]. According to these results shown in Table 8, it can be observed that the grain size increased with the increase in annealing time, bearing in mind that the increase in crystallite size in the samples is accompanied by an improvement in their electrical and optical properties as shown in Figure III.8.

3.2. Optical properties

Fig.2. indicates the transmittance spectra obtained for NiS at various annealing time. We notice that the transmittance rises with the wavelength increase and also increases with the annealing increase, owing to a rise in the thickness of deposited films. Because in the case of thicker films, there are more atoms in the films, and therefore there will be more cases of absorption of photons. We have found that the average optical transmittance for the deposited films is 0.56, 2.48, 5.63 and 6.09% for the films prepared at the following annealing time respectively: 0h, 1h, 2h and 3h.

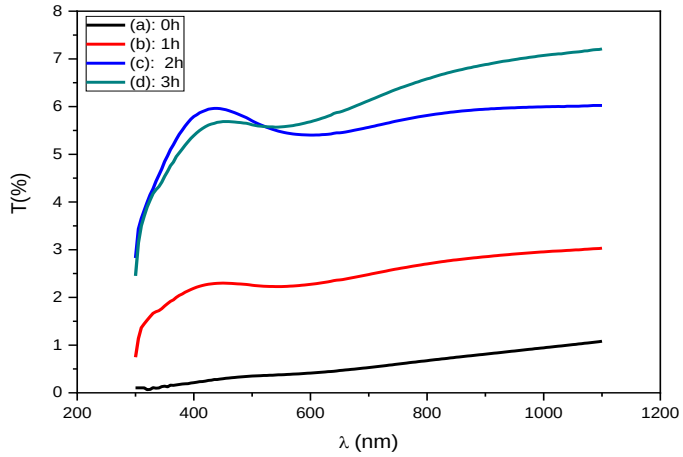

Fig. 2. Transmittance spectra of the NiS films: (a): 0h, (b): 1h, (c): 2h and (d): 3h.

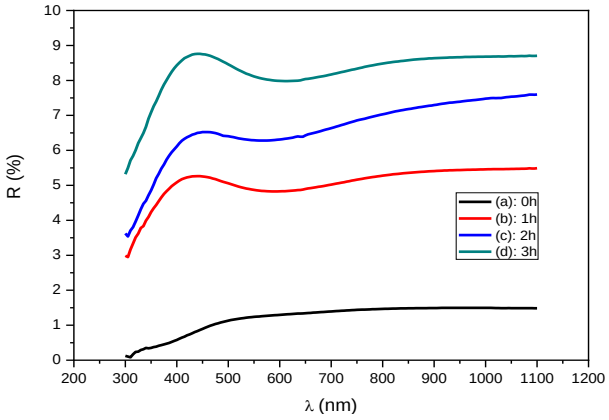

Fig. 3. Reflectance spectra of the NiS films: (a): 0h, (b): 1h, (c): 2h and (d): 3h.

Fig.3. shows the reflection spectra of NiS films prepared in different annealing times 0h, 1h, 2h and 3h. The figure indicates that the reflection increases with the annealing time increasing, owing to a rise in the thickness of deposited films. Because in the case of thicker films, there are more atoms in the films, and therefore there will be more cases of absorption of photons [25], and we have found that the average optical reflection of deposited films is 1.21, 5.06, 6.61 and 8.25 % films prepared at annealing time of 0h, 1h, 2h and 2h, respectively.

We also notice on the spectra of the reflectance that the value of the reflectance is always higher than the value of the transmittance, this phenomenon can be related to a metallic behavior, which reflects the absorbent character of the nickel sulfide film [3, 26].

From the transmittance and reflectance spectrum, the absorption coefficient (α) can be obtained from relation (10) [19].

$$\alpha = \frac{1}{e}\ln\left(\frac{(1-R)^2}{T}\right) \tag{12}$$

where: e is the film thickness, T is the transmittance, R is reflectance. In Fig. 4. We present the absorption coefficient variation (α) as a function of wavelength (λ) of deposited NiS films. We note a decrease in the value average of the absorption coefficient from 3.27×10^4, 2.59×10^4, 2.20×10^4 to 2.19×10^4 cm^{-1} for annealing time of 0, 1, 2 and 3h, respectively. This decrease can be correlated with improved crystal growth in NiS films by increasing annealing time, removal of defects and reduction in the number of grain boundaries. Moreover, the absorption coefficient values are close to the values of the literature [27].

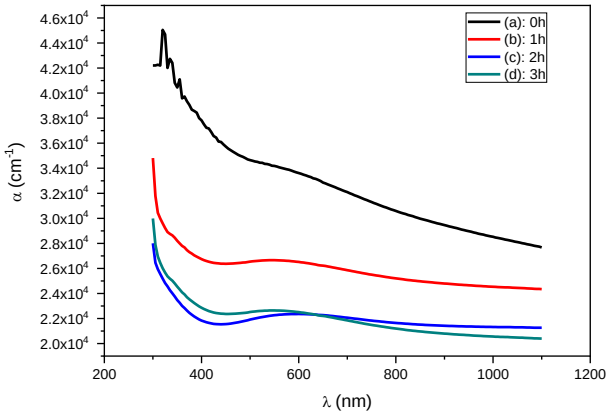

Fig. 4. Evolution of the absorption coefficient (α) of the NiS films: (a): 0h, (b): 1h, (c): 2h and (d): 3h.

The average value of absorption coefficient ($\langle\delta\rangle > 10^4$ cm^{-1}) for the films also supports the direct band gap nature of the film [27]. The films under study have an absorption coefficient (α) obeying the below relation for energies of high photon (hν) [28]:

$$\alpha h\nu = B\left(h\nu - E_g\right)^p \tag{13}$$

where: B is a constant; p is an integer which takes the value of 1/2 or 2 for the direct or indirect transitions, respectively. Fig. 5 shows the curves $(\alpha h\nu)^2$ versus energy (hν) for NiS thin films prepared at different annealing times 0h, 1h, 2h and 3h**.**

As seen in Fig. 5, a remarkable decrease in energy gap from 1.25 eV-1.01 eV was noticed by raising the annealing time from 0h to 3h, such a decrease may be due to the enhanced crystallinity with annealing time that resulted in the band gap that is optical varies with nickel to sulfur ratio in the structure leading to the change in the energy band structure, the states density (DOS) of the conduction band and the valence band [29].

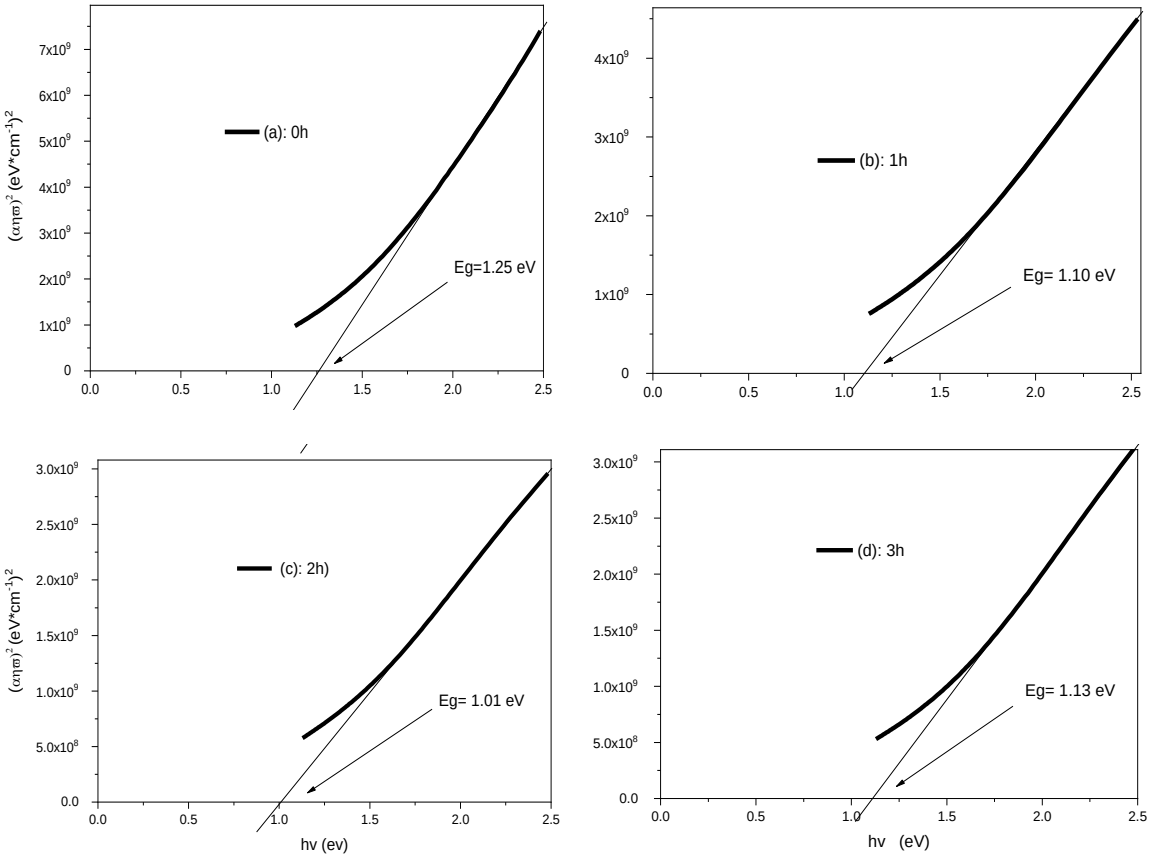

Fig. 5. $(ahv)^2$ vs. hv of the nanostructured NiS films: (a): 0h, (b): 1h, (c): 2h and (d): 3h.

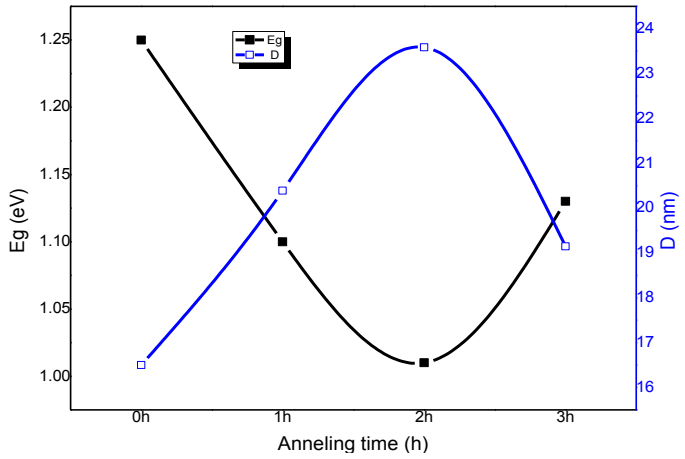

Fig. 6. Variation of the optical gap (Eg) and the grain size (D) as a function of the annealing time of the NiS films.

3.3. SEM & EDS

Figure 7 shows the surface morphology of NiS thin films deposited by the spray pyrolysis technique at substrate temperature 300 °C without annealing and annealed at 300 °C at different annealing times 0h, 1h, 2h and 3h.

From the SEM images of NiS deposited by the spray technique. We observed that the surface morphology of a NiS thin film deposited before annealing is fully covered, uniform and homogeneous and fuzzy. However, after annealing, the morphology of the layers that have not

undergone a thermal treatment reveals a difference in contrast between the unannealed film and annealed at 1h and 2h but in the time of annealing 3h it is noticed that the layer is darker, there are explosions of bubbles accompanied by ejection of material, this indicates that there is a formation in volume of a gas during the growth of the film which causes the emergence of bubbles on the surface, probably caused by the volatility of sulfur.

(a)

(b)

(c)

(d)

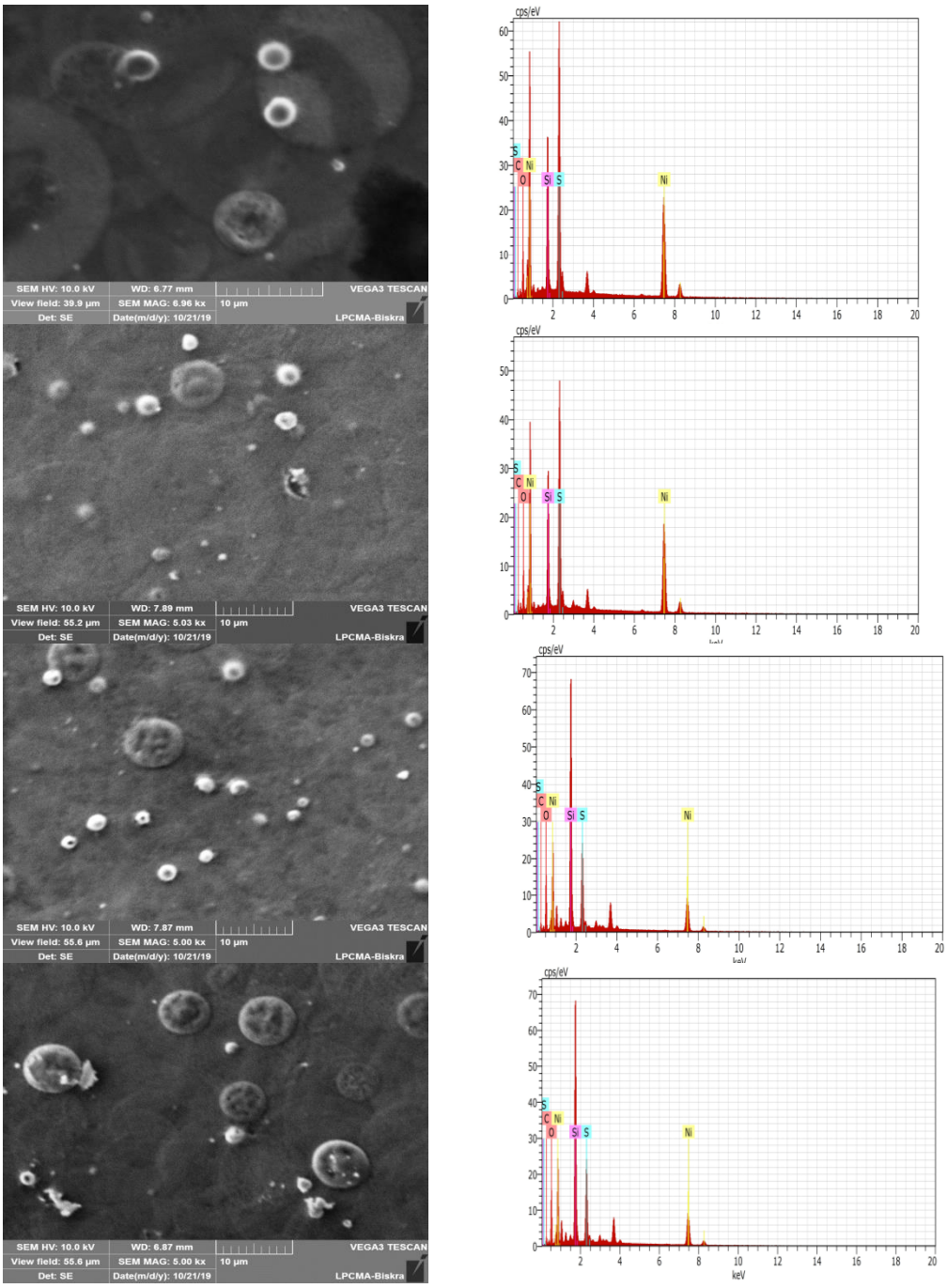

Fig. 7. SEM and EDS images for NiS thin films with different annealing times: (a) 0h, (b) 1h, (c) 2h and (d) 3h.

The EDS spectra of the films confirm the two elements Ni and S presence with different annealing time. Furthermore, the analysis showed the presence of other elements in the spectra such as oxygen (O) and silicon (Si) which originate from the SiO_2 glass substrate. While the presence of carbon C is probably due to thiourea ($SC(NH_2)_2$) involved in the synthesis. It is observed that the atomic percentage of sulfur decreases with the increase of the annealing time, we noted that the rate of sulfur is lower than that of nickel because sulfur is more volatile than nickel. Table. 9 summarizes the elementary analysis results.

Table 9. Elementary analysis of NiS thin films.

Annealing time	Ni (at. %)	S (at. %)	C (at. %)	O (at. %)	Si (at. %)	(Ni/S) (%)
(a): 0h	*23,79*	*21,59*	*20,85*	*21,73*	*12,05*	1.10
(b): 1h	*21,48*	*17,91*	*20,24*	*29,96*	*10,41*	1.19
(c): 2h	*18,47*	*16,24*	*26,17*	*25,42*	*25,42*	1.13
(d): 3h	*10,33*	*9,28*	*32,92*	*26,23*	*21,24*	1.11

3.4. Electrical properties

The electrical conductivity of NiS films is important for their application in supercapacitors. The electrical measurements of these films were made by the four point's technique. In table 10 we have reported the values of the square resistance (Rsh), resistivity (ρ) and conductivity (σ) measured from the four-point technique according to the following conditions. Plate shape: square, Insert size: 76.1 mm, Edge exclusion: 20 mm, Number of points: 4 points, Current used: 2.5312 mA.

The electrical conductivity of thin layers of NiS, it is based on the measured resistance of the sheet of the layers, as expressed [28].

$$R_{sh} = \frac{\pi}{ln2} \times \frac{V}{I} \tag{14}$$

$$\sigma = \frac{1}{\rho} = \frac{1}{e \times R_{sh}} \tag{15}$$

Table 10. Values of R_{sh}, ρ and σ of non-annealed and annealed NiS film 1h, 2h and 3h.

annealing time	R_{sh} (10^{-1} Ω/sq)	ρ (10^{-5} Ω.cm)	σ 10^4 $(\Omega.cm)^{-1}$
(a): 0h	1.63	2.81	3.56
(b): 1h	1.14	1.76	5.67
(c): 2h	8.28	1.26	7.91
(d): 3h	1.19	2.01	4.97

From the values recorded in Table 10, it can be seen that the conductivity increases according to the increase in the annealing time (0h, 1h and 2h). This conductivity value increase is explained by the increase in the size of the crystallites with an increase in the annealing time, because when the size of the crystals is large, the areas between the crystals will be small. At the level of these, there are complete bonds between the atoms, which stimulate the reduction of a large number of defects which are traps for free charges. These results obtained are close to the values found by the researcher [30, 31], Then at the time of 3 hours of annealing, we see that the conductivity drops to the value $4.97*10^4$ $(\Omega.cm)^{-1}$. The electrical conductivity decrease with the annealing time increase because of the increasing of the disorder in the films; consequently, the potential barriers are increased [32, 33] because the introduced atoms are segregated into the grain boundaries. These results are supported by DRX and EDS results as shown in Figure 8. These results suggest that the films prepared by the spray pyrolysis technique behave like a metal, which is evident from the results of the very high conductivity that exceeds 10^4 $(\Omega.cm)^{-1}$.

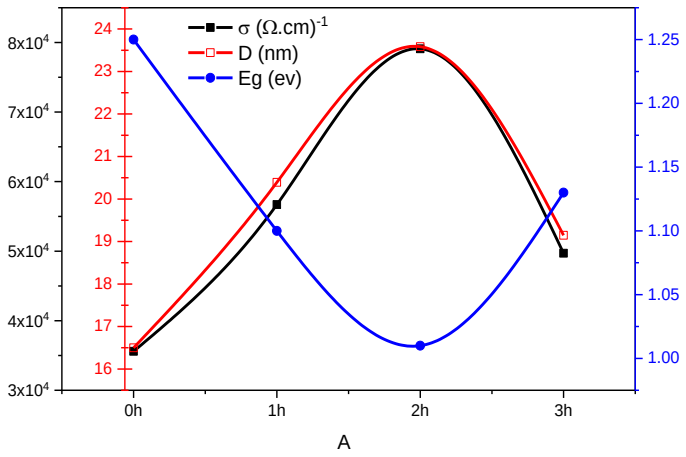

Fig. 8. Variation of conductivity, crystallite size and band gap of NiS films as a function of annealing time: 0h, 1h, 2h and 3h.

4. Conclusion

In this work we focused on the effect of annealing time on the morphological, optical, structural and electrical properties of nickel sulfide (NiS) thin films composed by spray pyrolysis deposited on glass substrates at the temperature of 300°C. Then, we discuss thermally treated in a temperature oven 300 °C at different times of 1 h, 2h and 3h. The diffraction of X-ray results indicated that the deposited NiS thin films are single-phase and polycrystalline, having the hexagonal structure with high intense peaks at the (012) orientations. The crystallite size was found to increase with increasing annealing time from 16.49 to 23.58 nm. The analysis of the optical properties showed that the band gap decreases from 1.25 to 1.01 eV for the 0h, 1h, 2h, and 3h annealing time, respectively. The coefficient order of the optical absorption is 10^4 cm^{-1}. The elemental composition analysis revealed that the atomic concentration of sulphur decreased with increasing annealing time. The SEM analysis showed that nanometer-sized spherical grains covering the entire surface of the films. Conductivity measurements through a four-point device showed that the conductivity increased with increasing annealing time from ($3.56*10^4$ to $7.91*10^4$ $(\Omega.cm)^{-1}$. The results obtained have shown that the prepared NiS films contain good crystallization, dense morphology, good stochiometric ratio and high conductivity, and these specifications make them a potential candidate as electrode material for application in super-capacitors.

Acknowledgments

Authors would like to thank Mr. Bali Hicham, a translator and a teacher of foreign languages for his help in writing this article.

References

[1] S. H. Yu, M. Yoshimura, Advanced Functional Materials 12(4), 277 (2002) ; https://doi.org/10.1002/1616-3028(20020418)12:4<277::AID-ADFM277>3.0.CO;2-M

[2] Y. Zhang, Z. Peng, S. Guan, X. Fu, Data in brief 16, 828 (2018) ; https://doi.org/10.1016/j.dib.2017.12.016

[3] A. Gahtar, S. Benramache, A. Ammari, A. Boukhachem, Annals of West University of Timisoara-Physics 63(1), 1(2021) ; https://doi.org/10.2478/awutp-2021-0001

[4] S. Suresh, S. S. Anand, R. Arul, D. Isha, Chalcogenide Letters 13(7), 291 (2016).

[5] A. Patil, A. Lokhande, P. Shinde, J. Kim, C. Lokhande, Journal of energy chemistry 27(3), 791 (2018) ; https://doi.org/10.1016/j.jechem.2017.05.005

[6] S. Sartale, C. Lokhande, Materials Chemistry and Physics 72(1), 101 (2001) ; https://doi.org/10.1016/S0254-0584(01)00314-5

[7] R. K. Singh, J. Narayan, Physical Review B 41(13), 8843 (1990) ; https://doi.org/10.1103/PhysRevB.41.8843

[8] H. Ruan, Y. Li, H. Qiu, M. Wei, Journal of Alloys and Compounds 588, 357 (2014) ; https://doi.org/10.1016/j.jallcom.2013.11.070

[9] P. Yang, M. Lü, C. F. Song, G. Zhou, D. Xu, D. R. Yuan, Journal of Physics and Chemistry of Solids 63(11), 2047 (2002) ; https://doi.org/10.1016/S0022-3697(02)00192-0

[10] V. P. Patil, S. Pawar, M. Chougule, P. Godse, R. Sakhare, S. Sen, P. Joshi, Journal of Surface Engineered Materials and Advanced Technology 01(02), 35 (2011) ; https://doi.org/10.4236/jsemat.2011.12006

[11] R. Karthikeyan, (2015).

[12] A. Ammari, M. Trari, B. Bellal, N. Zebbar, Journal of Electroanalytical Chemistry 823, 638 (2018) ; https://doi.org/10.1016/j.jelechem.2018.06.045

[13] V. Kumar, D. Sharma, K. Sharma, D. Dwivedi, Optik 156, 43 (2018) ; https://doi.org/10.1016/j.ijleo.2017.10.169

[14] B. Bharathi, S. Thanikaikarasan, P. Chandrasekar, P. Kollu, T. Mahalingam, L. Ixtlilco, Journal of New Materials for Electrochemical Systems 17(3), 167 (2014) ; https://doi.org/10.14447/jnmes.v17i3.417

[15] W. Chen, Y. Ning, Q. Li, K. Li, X. Wu, W. Wu, H. Zhang, Materials Letters XX, XXX (2018).

[16] M. Patel, I. Mukhopadhyay, A. Ray, Journal of Alloys and Compounds 619, 458 (2015) ; https://doi.org/10.1016/j.jallcom.2014.08.207

[17] C. Zaouche, Y. Aoun, S. Benramache, A. Gahtar, Scientific Bulletin of'Valahia'UniversityMaterials & Mechanics 17(17) (2019) ; https://doi.org/10.2478/bsmm-2019-0015

[18]. A. Gahtar, A. Rahal, B. Benhaoua, S. Benramache, Optik 125(14), 3674 (2014) ; https://doi.org/10.1016/j.ijleo.2014.01.078

[19] R. Boughalmi, A. Boukhachem, M. Kahlaoui, H. Maghraoui, M. Amlouk, Materials Science in Semiconductor Processing 26, 593 (2014) ; https://doi.org/10.1016/j.mssp.2014.05.059

[20] A. Gahtar, S. Benramache, A. Ammari, A. Boukhachem, A. Ziouche, Inorganic and Nano-Metal Chemistry 52(1), 112(2022) ; https://doi.org/10.1080/24701556.2020.1862225

[21] C. Buchmaier, M. Glänzer, A. Torvisco, P. Poelt, K. Wewerka, B. Kunert, K. Gatterer, G. Trimmel, T. Rath, Journal of Materials Science 52(18), 10898 (2017) ; https://doi.org/10.1007/s10853-017-1265-5

[22] A. Ammari, M. Trari, N. Zebbar, Materials Science in Semiconductor Processing 89, 97 (2019) ; https://doi.org/10.1016/j.mssp.2018.09.003
[23] W. Eidelloth, R. Sandstrom, Applied physics letters 59(13), 1632 (1991) ; https://doi.org/10.1063/1.106253
[24] N. K. Reddy, K. Ramesh, R. Ganesan, K. R. Reddy, K. Gunasekhar, E. Gopal, Applied Physics A 83(1), 133 (2006) ; https://doi.org/10.1007/s00339-005-3475-y
[25] K. Z. Yahiya, A. H. Jraiz, U. M. Nayef, Engineering and Technology Journal 26(7), 824 (2008).
[26] A. Gahtar, S. Benramache, C. Zaouche, A. Boukacham, A. Sayah, Advances in Materials Science 20(3), 36 (2020) ; https://doi.org/10.2478/adms-2020-0015
[27] A. Hammad, Z. Elmandouh, H. Elmeleegi, Acta Physica Polonica A 127(4), 901 (2015) ; https://doi.org/10.12693/APhysPolA.127.901
[28] A. Gahtar, S. Benramache, B. Benhaoua, F. Chabane, Journal of Semiconductors 34(7), 073002 (2013) ; https://doi.org/10.1088/1674-4926/34/7/073002
[29] S. Gedi, V. R. M. Reddy, C. Park, J. Chan-Wook, R. R. KT, Optical Materials 42, 468 (2015) ; https://doi.org/10.1016/j.optmat.2015.01.043
[30] M. G. Townsend, R. Tremblay, J. L. Horwood, L. J. Ripley, Journal of Physics C: Solid State Physics 4, 598 (1971) ; https://doi.org/10.1088/0022-3719/4/5/010
[31] J. Ray, M. Patel, P. Ghediya, TapasKChaudhuri, Mater. Res. Express 3, XXX (2016) ; https://doi.org/10.1088/2053-1591/3/7/075906
[32] A. Mosbah, M. Aida, Journal of Alloys and Compounds 515, 149 (2012) ; https://doi.org/10.1016/j.jallcom.2011.11.113
[33] M. Lucio-Lopez, M. Luna-Arias, A. Maldonado, M. d. l. L. Olvera, D. Acosta, Solar Energy Materials and Solar Cells 90(6), 733 (2006) ; https://doi.org/10.1016/j.solmat.2005.04.010